Influence of friction on imperfect conical indentation for elastoplastic material

J. P. Ponthot*[1], W. C. Guo[1,2], G. Rauchs[3] and W. H. Zhang[2]

The investigation of this paper provides a rationale of the influence of friction in nanoindentation testing for elastoplastic solids. The emphasis is placed on providing a detailed evaluation of the influence of the friction coefficient on the calculated hardness using an imperfect indenter. A new method for calculating the material hardness is derived. The new function can take into account the combined effects of friction and imperfect indenter tip geometry. For further investigations, some numerical simulations are executed. The results show that the new function can provide a good relationship for the hardness calculated in all friction cases. Moreover, the numerical simulations show that the friction coefficient does not significantly affect the curve of load versus indentation depth, whereas it significantly influences the deformations of the specimen surface around the indenter for some materials.

Keywords: Nanoindentation, Friction, Numerical simulation, Imperfect cone indenter, Material characterisation, Finite element method

Introduction

Nanoindentation is an increasingly popular technique for material characterisation at micro- and nanoscales. It has been developed in order to determine the hardness and Young's modulus for several decades. This test can be performed on a small bulk material and thin coating with a thickness <3 μm. At these scales, compression and tension tests cannot be performed. Moreover, it is important to be able to measure yield stress and hardening properties during such a test. As mentioned above, those advantages of indentation made this technique a powerful tool for evaluating the mechanical properties of materials.

An indentation instrument enables to register the indentation load P and indentation depth h simultaneously during the penetration of an indenter into a sample. Then, the hardness and Young's modulus are the main parameters that can be inferred from the $P-h$ curve. In a large number of publications, the material properties are evaluated through the indenter, which is assumed to exhibit a perfect geometric shape.[1,2] However, in practical indentation measurements, the indenter never has a perfect shape as designed, particularly for the indenter tip. Some uncertainties in nanoindentation measurements produced by the geometrical deviations of the indenter are significant. Especially at micro- or nanoscales (indentation depth, $h<0{\cdot}2$ μm), the geometrical deviations of the indenter exert a clearly larger influence on the uncertainty of hardness value than the influence quantities, which can be attributed to the measuring instrument.[3,4] In recent years, several corresponding investigations have been performed in order to find an effective method that can take into account the indenter tip geometries and material characteristics at the same time. For example, Antunes *et al.*[5] estimated the influences of the defect Vickers tips on the hardness and Young's modulus. The numerical results showed that large differences were obtained with different sizes of tip imperfections, and there were good agreements with experimental results. Bouzakis *et al.*[6] investigated the effect of indenter tip geometries on the accuracy of the stress–strain law determined using Berkovich and Vickers indenters. They pointed out that the indenters of the same type, but with different geometrical deviations for the indenter tips, can lead to obviously different nanoindentation results.

Besides the influence of the imperfect indenter tip, the effect of friction between indenter and specimen also should not be ignored, although many investigations resort to finite element simulations where, for simplicity, the influence of friction in the contact response has been neglected.[5,7–9] However, researchers have pointed out that friction plays an important role in contact problems for several decades. In 1985, Johnson *et al.*[10] studied the influence of friction in indentation by recourse to the slipline field theory. Such early investigations already indicated that an increase of up to 20% in hardness occurs for adhesive contacts compared to frictionless ones. In the authors' early studies, the maximum differences on hardness and Young's modulus can reach 14 and 7% respectively for some elastoplastic materials while neglecting friction.[11] More significantly, Mata *et al.*[12] showed that the values of yield stress and

[1]Aerospace and Mechanical Engineering Department, LTAS- MN[2]L, University of Liège, Liège, Belgium
[2]The Key Laboratory of Contemporary Design and Integrated Manufacturing Technology, Northwestern Polytechnical University, Xi'an, China
[3]Laboratoire de Technologies Industrielles, Centre de Recherche Public Henri Tudor, L-4221 Esch-sur-Alzette, Luxembourg

*Corresponding author, email JP.Ponthot@ulg.ac.be

Received 3 July 2009; accepted 17 November 2009
DOI 10.1179/175158309X12586382418418

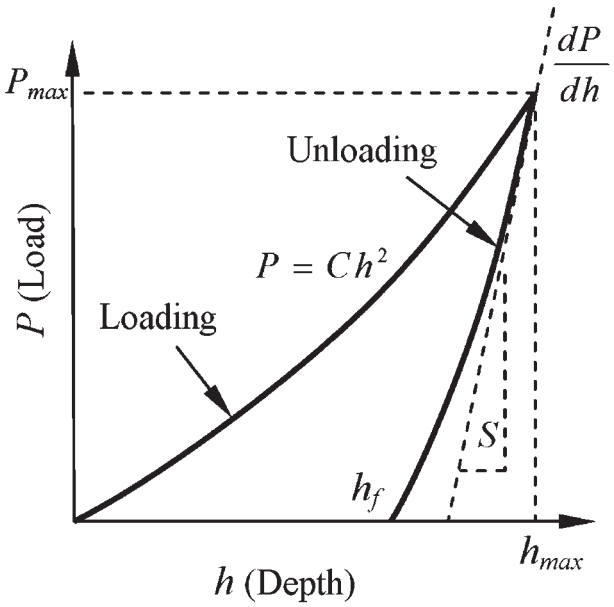

1 Schematic of load versus indentation depth curve

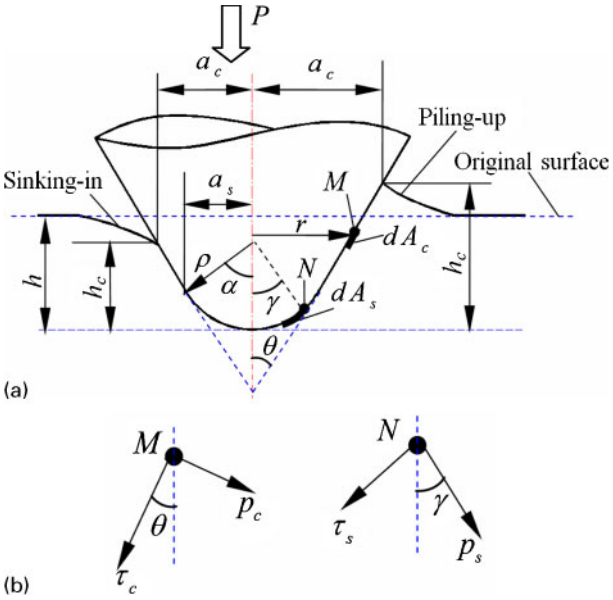

a geometrical structure of defect conical indenter; *b* forces on node, which is on spherical and conical surfaces respectively

2 Schematic of defect conical indentation profiles with sinking in and piling up

workhardening exponent, if extracted from the $P-h$ curves neglecting friction, may be overestimated by up to 50%.

From the above statements, it can be known that both the influences of the imperfect indenter tip geometry and the friction in the contact area cannot be neglected in nanoindentation measurements. Especially, the combined influences of them should be investigated. In the current published literature, few researchers have so far considered the influence of friction in nanoindentation with an imperfect indenter tip. Moreover, a theoretical background to evaluate the influence of the friction on sharp indentation measurement is still difficult to the authors' present knowledge due to its complex mechanical and mathematical nature. In this paper, a numerical study intends to contribute to a deeper understanding of the influence of friction in indentation with a defect indenter tip.

Theoretical framework

The indentation instrument can continuously register the load P versus the indentation depth h (see Fig. 1). By recording the data of the whole indentation procedure, the indentation hardness H can be calculated as suggested by Oliver *et al.*[13]

$$H = \frac{P}{A_{\text{proj}}} \tag{1}$$

where A_{proj} is the projected contact area. If the indenter is a cone (see Fig. 2*a*), it can be written as

$$A_{\text{proj}} = \pi a_c^2 \tag{2}$$

where a_c is the radius of the projected area produced by the conical indenter; θ is the half apex angle of the conical indenter. In practical applications, the indenters never have a possibility to have the perfect shapes as designed, and they always have a rounded tip. Normally, it is considered to be spherical[14] with the tip radius ρ (see Fig. 2*a*).

The influence of friction on contact stresses is analysed invoking the load equilibrium at the indenter's face. We can start by writing

$$P = \int_0^{\alpha} p(\gamma)\mathrm{d}A_s + \int_{a_s}^{a_c} p(r)\mathrm{d}A_c \tag{3}$$

The first term in equation (3) represents the force on the spherical surface part, and the second term represents the force on the conical surface part (see Fig. 2*b*), where

$$\mathrm{d}A_s = 2\pi\rho^2 \sin\gamma \mathrm{d}\gamma \tag{4}$$

$$\mathrm{d}A_c = 2\pi r \frac{\mathrm{d}r}{\sin\theta} \tag{5}$$

$$p(r) = \tau_c \cos\theta + p_c \sin\theta \tag{6}$$

$$p(\gamma) = \tau_s \sin\gamma + p_s \cos\gamma \tag{7}$$

Thus, equation (3) can be rewritten as

$$P = \int_0^{\alpha} (\tau_s \sin\gamma + p_s \cos\gamma) 2\pi\rho^2 \sin\gamma \mathrm{d}\gamma + \int_{a_s}^{a_c} (\tau_c \cos\theta + p_c \sin\theta) 2\pi r \frac{\mathrm{d}r}{\sin\theta} \tag{8}$$

If the Coulomb's friction model is considered between the interfaces of the indenter and the specimen, over the contact regions, it is can be described as

$$\tau_s = \mu p_s \tag{9}$$

$$\tau_c = \mu p_c \tag{10}$$

According to equations (9) and (10), equation (8) becomes

$$P = \int_0^{\alpha} (\mu \sin\gamma + \cos\gamma) p_s(\gamma) 2\pi\rho^2 \sin\gamma \mathrm{d}\gamma + \int_{a_s}^{a_c} (\mu \cos\theta + \sin\theta) p_c(r) \frac{2\pi r}{\sin\theta} \mathrm{d}r \tag{11}$$

Hence, the hardness can be rearranged as

$$H=\frac{P}{A_{\text{proj}}}$$
$$=\frac{2}{a_c^2}\left[\int_0^{\alpha}(\mu\sin\gamma+\cos\gamma)p_s(\gamma)\rho^2\sin\gamma\,d\gamma+\int_{a_s}^{a_c}(\mu\cos\theta+\sin\theta)p_c(r)\frac{r}{\sin\theta}dr\right] \quad (12)$$

In the literature, most researchers generally do not consider the friction in the contact regions.[5,7–9] The hardness H_o can be obtained through the integrated contact pressure at the contact regions for $\mu=0$. Then, equation (12) can be written in a simple form

$$H=H_o+\lambda_o\mu \quad (13)$$

where

$$H_o=\frac{2}{a_c^2}\left[\int_0^{\alpha}\sin\gamma\cos\gamma p_s(\gamma)\rho^2 d\gamma+\int_{a_s}^{a_c}p_c(r)r dr\right] \quad (14)$$

$$\lambda_o=\frac{2}{a_c^2}\left[\int_0^{\alpha}\rho^2\sin^2\gamma p_s(\gamma)d\gamma+\int_{a_s}^{a_c}p_c(r)r\cot\theta dr\right] \quad (15)$$

While $r\leqslant a_s$, the relation of r and γ is given by

$$r=\rho\sin\gamma \quad (16)$$

Thus, equation (15) can be replaced by

$$\lambda_o=\frac{2}{a_c^2}\left[\int_0^{a_s}p_s(r)\frac{r^2}{(\rho^2-r^2)^{1/2}}dr+\int_{a_s}^{a_c}p_c(r)r\cot\theta dr\right] \quad (17)$$

Numerical simulations

Materials

The materials used in the numerical simulations are listed in Table 1. For these elastoplastic models, the Young's modulus of material is represented as E, and the initial yield stress is represented as σ_y. In general, the true stress–true strain $\sigma-\varepsilon$ curves of elastoplastic engineering metals can be closely approximated by the power law description:[10,15,16]

$$\sigma=\begin{cases}E\varepsilon, & \text{for}\quad \sigma\leqslant\sigma_y\\ R\varepsilon^n, & \text{for}\quad \sigma\geqslant\sigma_y\end{cases}. \quad (18)$$

where n is the workhardening exponent, and R is the workhardening rate which can be calculated as

$$R=\frac{E^n}{\sigma_y^{n-1}} \quad (19)$$

In the following numerical calculations, the Poisson's ratio is designated by v, and von Mises plasticity with J_2 flow theory is assumed. With the above assumptions and definitions, four independent parameters (E, v, σ_y and n) are required to completely characterise the elastoplastic properties of the testing materials. The materials used in the following parts are listed in Table 1.

Table 1 Materials used in simulations

Name	(E, v, σ_y, n)
SAF 2507 stainless steel[12]	(200 GPa, 0·3, 675 MPa, 0·19)
Annealed copper[12]	(110 GPa, 0·32, 20 MPa, 0·52)
Aluminium alloy[17]	(70 GPa, 0·3, 500 MPa, 0·122)

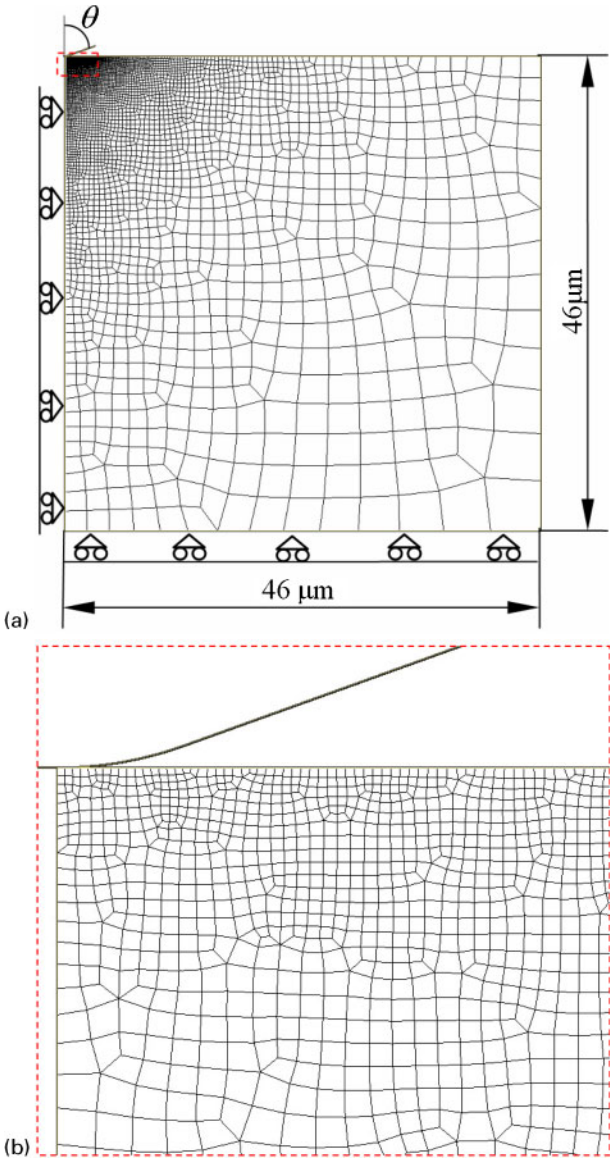

a complete mesh; *b* details of contact region

3 Two-dimensional axisymmetric model with defect conical indenter

Computational models

All numerical simulations are performed using METAFOR,[18] which is a finite element code developed at the University of Liège. The two-dimensional axisymmetric finite element model constructed to simulate the indentation responses of elastoplastic solids is shown in Fig. 3. The finite element model is modelled using 6428 four-node quadrilateral elements, with a finer mesh near the contact region and a gradually coarser mesh further away from the contact region (see details in Fig. 3*b*) ensuring for the numerical accuracy. In Fig. 3*a*, the axis of symmetry is on the left side of the model, and the displacements of the nodes on this boundary are constrained in the horizontal direction. The displacements of the nodes on the bottom side are constrained in the vertical direction.

For all simulations, the half apex angle of the cone is defined as $\theta=70{\cdot}3^\circ$, the tip radius of the conical indenter

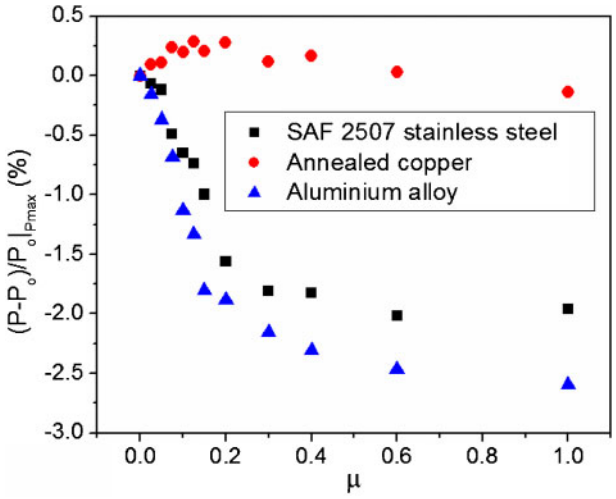

4 Difference of P_{max} compared to frictionless case μ=0·0

is assumed as ρ=0·5 μm. The load is performed by controlling the displacement of the indenter, and the maximum penetration depth is set as h_{max}=0·7 μm. At maximum load, more than 135 nodes are in contact. The size of specimen is 46×46 μm, which is at least 30 times larger than the size of the imprint produced by the indenter at peak load and guarantees that the simulation results are not affected by the boundaries.

Results and discussion

Effects on *P*−*h* curves

The $P-h$ curves obtained with varying friction coefficient μ for the three materials listed in Table 1 are nearly identical. For example, for the maximum difference of P_{max} compared to the frictionless case μ=0·0, it equals 2·59% and appears in the simulation for aluminium alloy. For annealed copper, it is only 0·28% (see Fig. 4). Therefore, it can be said that the $P-h$ curves are almost identical for all friction coefficients.

Simultaneously, the surface deformations of the specimen around the indenter for SAF 2075 stainless steel are shown in Fig. 5. Notice that for small μ, piling up takes place. With an increase in μ, piling up becomes insignificant and even disappears, e.g. in the cases of

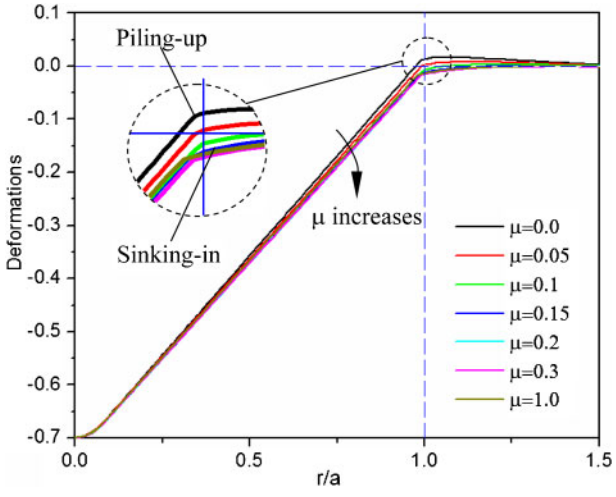

5 Surface deformation of specimen around indenter for SAF 2075 stainless steel

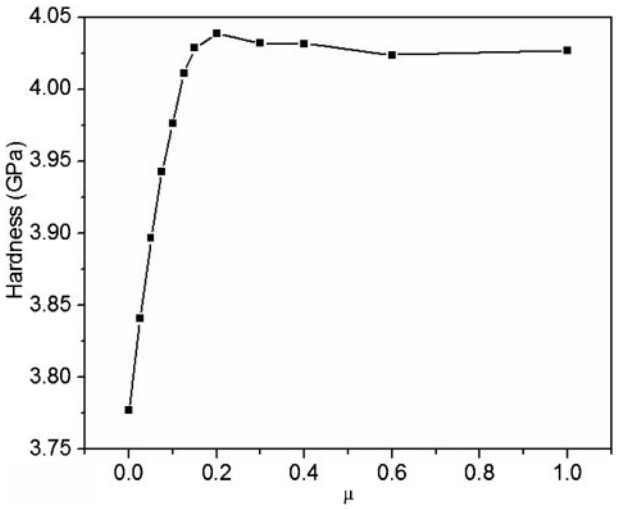

6 Hardness versus friction coefficient for SAF 2075 stainless steel. Maximum difference of hardness reaches to 6·93%

μ>0·05. At the same time, sinking in increases with an increase in μ. This tendency leads the projected contact area A_{proj} to decrease with an increase in μ. If follows that the hardness H, which is calculated by equation (1), will increase. For example, the corresponding calculated hardness for SAF 2507 stainless steel can be seen in Fig. 6. It is clearly seen that the hardness increases with an increase in μ while μ<0·2. The maximum difference of the calculated hardness is ~6·93% compared to the frictionless case. While μ>0·2, it seems that the calculated hardness is constant. Figure 5 shows that the surface deformations of the specimen around the indenter are also nearly identical while μ>0·2. When the displacements of nodes in the contact area are studied, it can be found that while μ is large, the nodes on the interfaces have a tendency to adhere to the indenter. This means the friction coefficient does not affect the simulation results when it is large and will lead nearly the same results. A similar consequence was also obtained in the authors' early studies with sharp conical indenter.[11] However, the influence of friction is significant for the calculated hardness, especially for small μ. Thus, in the following parts, the authors mainly investigate the effect of friction on calculated hardness with the assumption that μ only varies in the range of 0–0·15.

Effect on pressure distribution

A fundamental understanding of the effect of friction in the contact area can be gained by comparing the distributions of contact pressure $p(r)$ for frictional contacts with different friction coefficients. The effects on normalised pressure distributions are shown in Fig. 7. In the spherical contact zone ($r/a_c \leqslant 0{\cdot}0868$), the distributions of the normalised pressures exhibit a peak. On the other hand, in the conical contact part ($0{\cdot}0868 < r/a_c \leqslant 1{\cdot}0$), the distributions of normalised pressures decrease from r/a_c=0·0868 towards the contact boundary r/a_c=1·0. The normalised pressures in the spherical contact zone first increase and then decrease with an increase in μ. The normalised pressures in the conical contact zone increase with an increase in μ, and the distributions of the normalised pressures tend to be flatted.

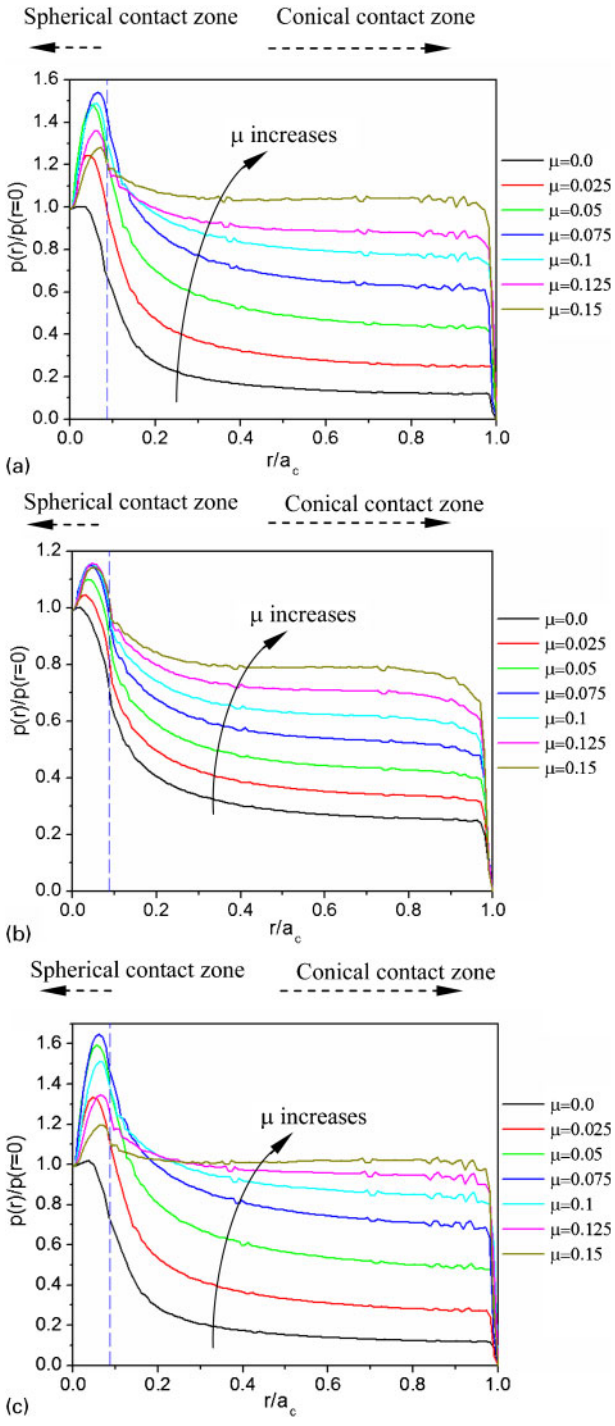

a SAF 2507 stainless steel; *b* annealed copper; *c* aluminium alloy

7 Influence of the friction coefficient on normalised pressure distributions

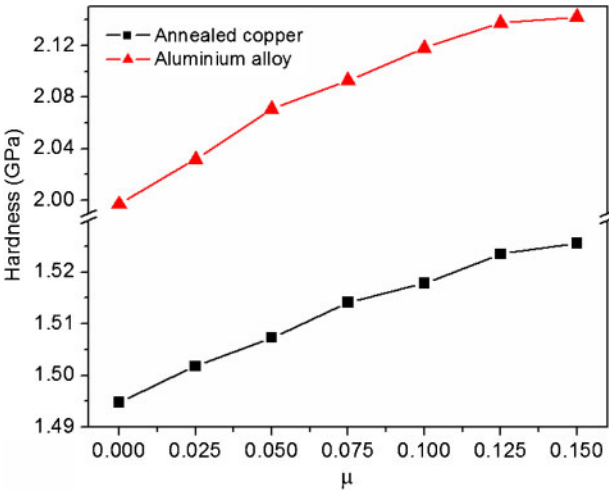

8 Hardness versus friction coefficient for annealed copper and aluminium alloy

Effects on hardness

The hardness calculated by equation (1) are shown in Fig. 8 for the other two materials. As expected, the hardness also increases following an increase in the friction coefficient. As stated before, the hardness can also be calculated by equation (13). Herein, the calculated value of λ_o equals 2·24, 0·75 and 1·15 respectively for SAF 2507 stainless steel, annealed copper and aluminium alloy. The corresponding results compared with those obtained by equation (1) are listed in Table 2. It is noted that the hardness obtained by these two methods is in good agreement. The differences of the hardness obtained by the two methods are lower than 5%. This means that equation (13) can provide a good relationship between H and H_o. Moreover, according to equation (13), the relative variation between H and H_o can be described as

$$\mathrm{Var} = \frac{H - H_o}{H_o} 100\% = \frac{\lambda_o \mu}{H_o} 100\% \qquad (20)$$

Therefore, comparing with the frictionless case, the maximum difference of hardness load by friction coefficient can reach 8·99, 7·55 and 8·62% respectively for the three materials (see Table 2).

Effects on plastic flow

According to equation (2), the projected contact area A_{proj} is dependent on the radius of projected area a_c, and the contact radius a_c has a direct relation to the surface deformations of the specimen around the indenter. On the one hand, if the surface deformations are piling-up, A_{proj} will be larger, and the calculated hardness H will be

Table 2 Calculated hardness, GPa

	SAF 2507 stainless steel			Annealed copper			Aluminium alloy		
μ	Equation (1)	Equation (13)	Diff, %	Equation (1)	Equation (13)	Diff, %	Equation (1)	Equation (13)	Diff, %
0	3·78	3·78	0·00	1·49	1·49	0·00	2·00	2·00	0·00
0·025	3·82	3·84	0·42	1·50	1·51	0·58	2·02	2·03	0·43
0·05	3·86	3·90	0·83	1·51	1·53	1·16	2·05	2·06	0·37
0·075	3·90	3·95	1·23	1·51	1·55	2·40	2·07	2·09	0·79
0·1	3·94	4·00	1·62	1·52	1·57	2·96	2·10	2·12	0·71
0·125	3·99	4·06	1·75	1·52	1·58	4·19	2·12	2·14	1·12
0·15	4·03	4·12	2·13	1·53	1·60	4·74	2·15	2·17	1·05

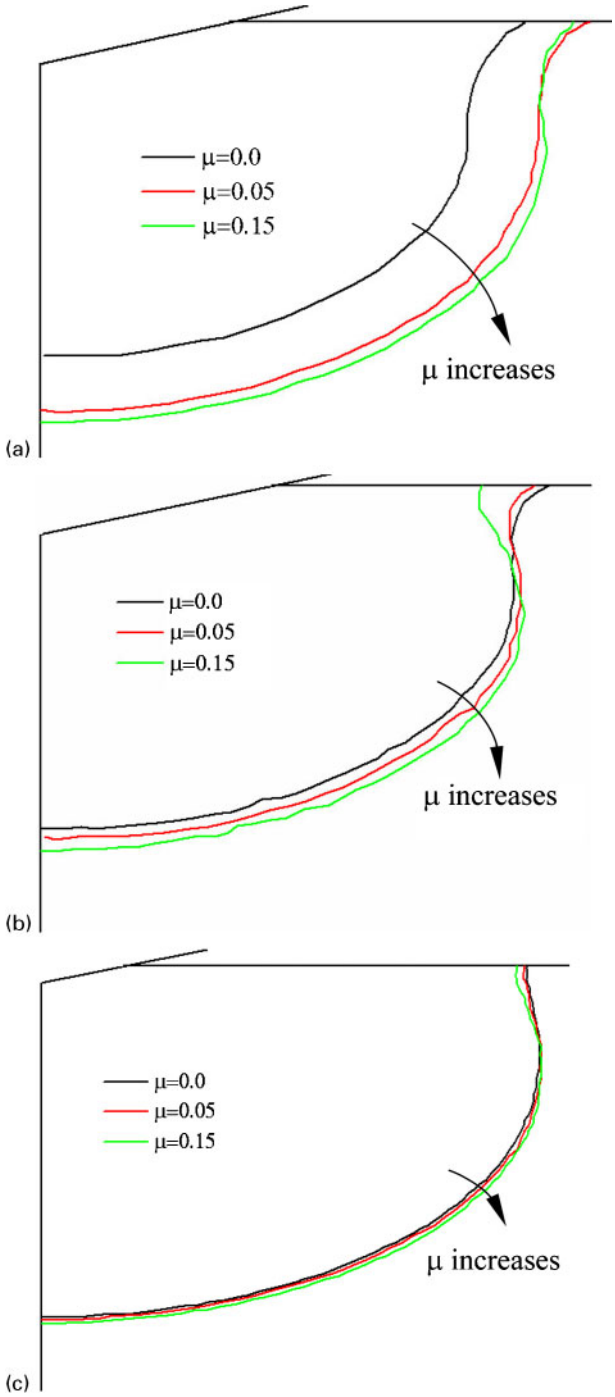

a SAF 2507 stainless steel; *b* aluminium alloy; *c* annealed copper

9 Plastic zone size increases as function of μ

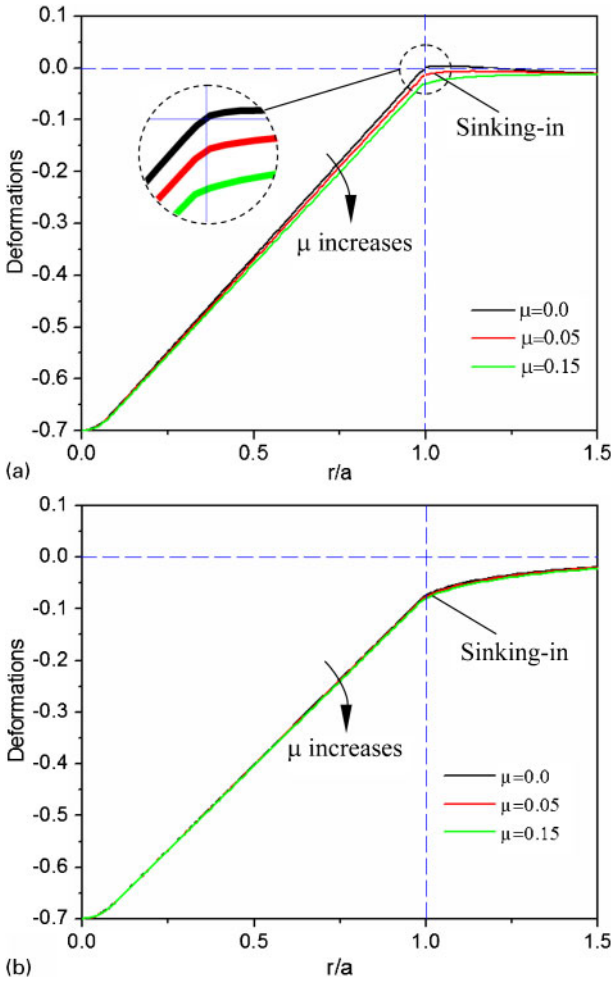

a aluminium alloy; *b* annealed copper

10 Surface deformation of specimen around indenter

smaller. On the other hand, if the surface deformations are sinking in, H will be larger since A_{proj} is smaller. Indeed, the surface deformations highly depend on the plastic flow. For example, piling-up develops as a result of large outward flow at the interface. Hence, it is necessary to investigate the motion of the material between the indenter and the specimen. The effects of friction coefficient on plastic zone size are shown in Fig. 9. The motions of plastic flows are promoted in radial direction with an increasing friction coefficient. The increase in μ brings significant changes compared to the frictionless case for SAF 2507 stainless steel. However, for the other two materials, the plastic zone sizes do not enlarge significantly with an increasing μ. Especially for annealed copper, the increase is inconspicuous.

The surface deformations of the specimen around the indenter are shown in Figs. 5 and 10. For SAF 2507 stainless steel, the surface deformations change from piling-up to sinking-in with an increasing μ. For aluminium alloy, either piling-up or sinking-in appears in the absence of friction. With an increase in μ, sinking in becomes dominant. For annealed copper, sinking in is always exhibited and nearly identical, although μ varies from 0 to 0·15. Therefore, it can be said that the influence of friction on surface deformation is significant in the materials where piling-up occurs. However, frictional constraints have little influence in the material where sinking in already occurs in the absence of friction. This also explains the small difference (only 0·28% in Fig. 4*b* and 2.06% in Fig. 8) in the $P-h$ curves and calculated hardness of annealed copper.

Moreover, it is also noticed that, for the three materials, the plastic zones do not expand but reduce near the surface of specimen when μ=0·15. While the friction coefficient has a large value, the material tends to adhere to the indenter. When the indenter penetrates into the solids, the corresponding motions near the surface have a tendency of moving close to the indenter, whereas the material under the indenter still tends to move in radial direction.

Conclusions

The present investigation provides a rationale of the influence of friction in the imperfect conical nanoindentation of elastoplastic solids. The emphasis is placed on providing a detailed evaluation of the influence of the friction coefficient μ on the calculated hardness. Equation (13), which is modified from Oliver's hardness equation, provides an explicit relation between H and H_o in theory and can be used to account for the combined effects of friction coefficient and the indenter tip geometry. The numerical simulation results show that the friction coefficient μ does not influence the $P-h$ curves significantly. However, the influence on the calculated hardness is remarkable for some materials. From the further investigations about the pressure distribution and plastic flow, it is clearly seen that the normalised pressure in the spherical contact area with an increase in μ first increases while $\mu<0{\cdot}075$ and then decreases while $\mu>0{\cdot}075$. In the conical contact area, it increases, and the distributions of the normalised pressures tend to be flatted with an increasing μ. At the same time, the motions of plastic flow are promoted in radial direction with an increasing friction coefficient for the materials where piling-up occurs in the absence of friction. For the materials where sinking-in already occurs in the absence of friction, joint motions between the indenter and the specimen seem to have a less relation to the value of the friction coefficient.

Acknowledgements

The authors would like to gratefully acknowledge the financial support from Ministère de la Culture, de l'Enseignement Supérieur et de la Recherche (MCESR) of the Grand Duchy of Luxembourg under the grant no. BFR 06/027 and the support from the 111 project (grant no. B07050) of China.

References

1. J. Luo and J. Jin: 'A study on the determination of plastic properties of metals by instrumented indentation using two sharp indenters', *Int. J. Solids Struct.*, 2007, **44**, 5803–5817.
2. T. A. Venkatesh: 'Determination of elasto-plastic properties by instrumented sharp indentation: guidelines for property extraction', *Scr. Mater.*, 2000, **42**, 833–839.
3. K. Herrmann, K. Hasche, F. Pohlenz and R. Seemann: 'Characterisation of the geometry of indenters used for the micro- and nanoindentation method', *Measurement*, 2001, **29**, 201–207.
4. J. Zhang and M. Sakai: 'Geometrical effect of pyramidal indenters on the elastoplastic contact behaviors of ceramics and metals', *Mater. Sci. Eng. A*, 2004, **A381**, 62–70.
5. J. M. Antunes, L. F. Menezes and J. V. Fernandes: 'Influence of Vickers tip imperfection on depth sensing indentation tests'. *Int. J. Solids Struct.*, 2007, **44**, 2732–2747.
6. K. D. Bouzakis, N. Michailidis, S. Hadjiyiannis, G. Skordaris and G. Erkens: 'The effect of specimen roughness and indenter tip geometry on the determination accuracy of thin hard coatings stress–strain laws by nanoindentation', *Mater. Charact.*, 2003, **49**, 149–156.
7. W. Y. Yan, Q. P. Sun, X. Q. Feng and L. M. Qian: 'Analysis of spherical indentation of superelastic shape memory alloys', *Int. J. Solids Struct.*, 2007, **44**, 1–17.
8. J. M. Solberg, R. E. Jones and P. Papadopoulos: 'A family of simple two-pass dual formulations for the finite element solution of contact problems', *Comput. Methods Appl. Mech. Eng.*, 2007, **196**, 782–802.
9. S. W. Youn and C. G. Kang: 'FEA study on nanodeformation behaviors of amorphous silicon and borosilicate considering tip geometry for pit array fabrication', *Mater. Sci. Eng. A*, 2005, **A390**, 233–239.
10. K. L. Johnson: 'Contact mechanics'; 1985, Cambridge, Cambridge University Press.
11. W. C. Guo, G. Rauchs, W. H. Zhang and J. P. Ponthot: 'Influence of friction in material characterization in microindentation measurement', *Journal of Computational and Applied Mathematics*. In Press, corrected proof available online.
12. M. Mata and J. Alcala: 'The role of friction on sharp indentation', *J. Mech. Phys. Solids*, 2004, **54**, 145–165.
13. G. Oliver and G. M. Pharr: 'An improved technique for determining hardness and elastic modulus using load and displacement sensing indentation experiments', *J. Mater. Res.*, 1992, **7**, 1564–1583.
14. A. C. Fischer-Cripps: 'Nanoindentation'; 2002, Berlin, New York, Springer-Verlag.
15. M. Dao, N. Chollacoop, K. J. van Vliet, T. A. Venkatesh and S. Suresh: 'Computational modeling of the forward and reverse problems in instrumented sharp indentation', *Acta Mater.*, 2001, **49**, 3899–3918.
16. X. Chen, N. Ogasawara, M. H. Zhao and N. Chiba: 'On the uniqueness of measuring elastoplastic properties from indentation: the indistinguishable mystical materials', *J. Mech. Phys. Solids*, 2007, **55**, 1618–1660.
17. J. L. Bucaille, S. Stauss, E. Felder and J. Michler: 'Determination of plastic properties of metals by instrumented indentation using different sharp indenters', *Acta Mater.*, 2003, **51**, 1663–1678.
18. J. P. Ponthot: 'Finite element code: METAFOR', available at: http://metafor.ltas.ulg.ac.be/dokuwiki/